

## POLARIZED FAR-INFRARED AND SUBMILLIMETER EMISSION FROM INTERSTELLAR DUST

BRUCE T. DRAINE AND AURÉLIEN A. FRAISSE

Princeton University Observatory, Peyton Hall, Princeton, NJ 08544, USA

*Draft version September 7, 2008*

### ABSTRACT

Polarized far-infrared and submillimeter emission is calculated for models of nonspherical dust grains that are constrained to reproduce the observed wavelength-dependent extinction and polarization of starlight. For emission from regions where the magnetic field is perpendicular to the line-of-sight, the far-infrared emission is expected to have substantial linear polarization at wavelengths  $\lambda \gtrsim 100 \mu\text{m}$ , but the degree of linear polarization, and its variation with wavelength, is model-dependent. Models in which the starlight polarization is produced by both amorphous silicate and graphite grains have linear polarizations between 6% and 10% at  $\lambda > 100 \mu\text{m}$ , but for some models in which only silicate grains are spheroidal, the linear polarization increases from about 3% at  $100 \mu\text{m}$  to about 15% at 1 mm. We briefly discuss the implications of these results for removal of the polarized dust emission from maps of the Cosmic Microwave Background, as well as the possibility of discriminating among interstellar dust models based on observations of far-infrared and submillimeter linear polarization.

*Subject headings:* radiation mechanisms: thermal — dust, extinction — infrared: ISM

### 1. INTRODUCTION

The presence of dust grains in the interstellar medium has been apparent since the recognition that obscuring material existed in at least some regions of interstellar space (Barnard 1907, 1910; Trumpler 1930). Our knowledge of interstellar dust has advanced considerably since then, but remains incomplete [see, e.g., the review by Draine (2003), or the book by Whittet (2003)].

In the Milky Way, large fractions of abundant elements, such as Si and Fe, appear to have been depleted from the gas phase (Jenkins 2004), with the missing atoms believed to be present in dust grains. Studies of interstellar “reddening” produced by wavelength-dependent extinction revealed broad spectroscopic features at  $9.8 \mu\text{m}$  and  $18 \mu\text{m}$ , attributed to amorphous silicate material in submicron particles, and a strong extinction “bump” at  $2175 \text{ \AA}$ , usually attributed to aromatic carbon, perhaps graphite or polycyclic aromatic hydrocarbons (PAHs), in particles with radii  $a \lesssim 0.01 \mu\text{m}$ . Another broad extinction feature, at  $3.4 \mu\text{m}$ , is typical of C-H stretching modes in hydrocarbons. Finally, the observed infrared emission from dust includes spectral features at  $3.3$ ,  $6.2$ ,  $7.7$ ,  $8.6$ ,  $11.3$  and  $12.7 \mu\text{m}$  that can be explained by a substantial population of particles with PAH composition and sizes extending down to about 40 atoms.

These spectroscopic features indicate that amorphous silicates and carbonaceous materials, including PAHs, contribute a substantial fraction of the interstellar grain mass, and models developed to try to reproduce the observed extinction using observed abundances of the elements invariably employ amorphous silicates and carbonaceous materials as their main components.

The serendipitous discovery (Hiltner 1949; Hall 1949) of the linear polarization of starlight demonstrated that interstellar grains are both appreciably nonspherical and aligned with the interstellar magnetic field, so that the dusty interstellar medium acts as a polarizer. Studies

of starlight polarization in the ultraviolet (Clayton et al. 1992; Anderson et al. 1996; Martin et al. 1999) indicate that the smallest dust grains are apparently minimally aligned (Kim & Martin 1995), and studies in the infrared [see, e.g., Whittet (2003)] find strong polarization in the  $9.8 \mu\text{m}$  Si-O stretch absorption feature, requiring that a substantial fraction of the amorphous silicate particles be aligned. Recent measurements of the polarization in the neighborhood of the  $3.4 \mu\text{m}$  C-H stretch absorption feature (Chiar et al. 2006) find only upper limits on possible polarization associated with the feature, indicating that the hydrocarbon material responsible for this feature is primarily in a grain population that is not appreciably aligned, which may rule out models where the hydrocarbon material is located in mantles coating silicate cores.

While we know for sure that interstellar grains are not spherically symmetric, their actual shapes are uncertain. Because the degree of alignment is unknown, we can only say that the grains must depart from spherical symmetry sufficiently to produce the observed polarization.

Interstellar grains radiate strongly in the far-infrared. Because the grains are nonspherical and partially aligned, this emission must be partially polarized. The polarization of the far-infrared emission has been measured for infrared-bright regions in star-forming molecular clouds (see the review by Hildebrand 2005). The degree of polarization of the thermal emission from dust in these regions is observed to have a complicated wavelength dependence, with the polarization at  $350 \mu\text{m}$  observed to be significantly smaller than the  $100 \mu\text{m}$  and  $850 \mu\text{m}$  polarization (Vaillancourt 2002; Hildebrand & Kirby 2004; Hildebrand 2005; Vaillancourt 2007), which has been interpreted as indicating two separate populations of emitting grains in these clouds.

The polarization of the large-scale submillimeter emission from dust in the interstellar medium of the Milky Way has now been measured by several experiments, including the Archeops balloon (Benoît et al. 2004; Ponthieu et al. 2005) and the WMAP satellite (Page et al. 2007; Gold et al. 2008). A quantitative un-

derstanding of this emission is important for removal of polarized Galactic “foregrounds” from maps of the cosmic microwave background (CMB), but also offers an opportunity to test models for interstellar grains.

In this paper, we construct models of interstellar dust that are consistent with the observed wavelength-dependent interstellar extinction, and the observed linear dichroism of the interstellar medium. We will calculate the polarized infrared and submillimeter emission from different models of interstellar dust heated by the general interstellar starlight, and, for each of them, compute the corresponding expected percentage polarization. This will allow us to gain a sense of the degree to which the predicted far-infrared polarization is model-dependent.

We discuss the observed wavelength-dependent extinction and polarization of starlight in §2, and the basics of the dust models we consider in §3. §4 provides a description of the technique we use to compute optical cross sections, while §5 introduces the formalism associated with “picket-fence” alignment. In §6, we present the size distributions and alignment functions that provide the best fit to the observed extinction and polarization discussed in §2. We describe the formalism we use to calculate the partially-polarized far-infrared emission by interstellar dust in §7. The corresponding results are presented and discussed in §8. Finally, §9 offers a summary of the main results of this paper, and a brief discussion of their consequences for studies of the CMB.

## 2. EXTINCTION AND POLARIZATION OF STARLIGHT

The grain models considered here will be required to reproduce the observed extinction by interstellar dust. Gas and dust are generally well-mixed, and the mixture is characterized by the observed extinction cross section at wavelength  $\lambda$  per H nucleon

$$\sigma_{\text{ext}}^{(\text{obs})}(\lambda) \equiv 0.4 (\ln 10) \frac{A_\lambda / \text{mag}}{N_{\text{H}}}, \quad (1)$$

where  $A_\lambda$  is the measured extinction, and  $N_{\text{H}}$  the column density of H nucleons. In diffuse sightlines,  $N_{\text{H}}$  can be determined from ultraviolet observations of Lyman- $\alpha$  absorption by atomic H and Lyman- and Werner-band absorption from  $\text{H}_2$ . The extinction produced by dust in the diffuse interstellar medium has been studied from about  $0.1 \mu\text{m}$  to slightly over  $10 \mu\text{m}$  [see, e.g., the review by Fitzpatrick (2004)]. At wavelengths  $4 \lesssim \lambda \lesssim 8 \mu\text{m}$ , the extinction is somewhat controversial (Lutz et al. 1996; Rosenthal et al. 2000; Indebetouw et al. 2005; Flaherty et al. 2007), but the present study will be limited to the wavelength range  $0.1 < \lambda < 2.65 \mu\text{m}$ , where the extinction by dust in diffuse regions appears to be securely known. We take the wavelength dependence of the observed extinction to be given by the Fitzpatrick (1999) parametrization for  $R_V \equiv A_V / (A_B - A_V) = 3.1$ , and, following Bohlin et al. (1978), the value of  $N_{\text{H}} / (A_B - A_V)$  is set to  $5.8 \times 10^{21} \text{ cm}^{-2} / \text{mag}$ .

The light emitted by stars is usually unpolarized, and the observed fractional polarization is produced by linear dichroism of the interstellar medium – a difference in the attenuation between two orthogonal linear polarization modes. We define the fractional polarization

$$p \equiv \frac{F_1 - F_2}{F_1 + F_2} = \frac{e^{-\tau_1} - e^{-\tau_2}}{e^{-\tau_1} + e^{-\tau_2}} = \tanh(\Delta\tau), \quad (2)$$

where  $\Delta\tau \equiv (\tau_2 - \tau_1)/2$ ,  $F_1$  and  $F_2$  are the fluxes in each of two orthogonal polarization modes, and  $\tau_1$  and  $\tau_2$  the extinctions for these modes. The observed polarization fraction  $p(\lambda)$  tends to peak at a wavelength  $\lambda_{\text{max}}$  between about  $0.5$  and  $0.9 \mu\text{m}$ , with the larger values of  $\lambda_{\text{max}}$  coming from sightlines through dense clouds; diffuse cloud sightlines tend to have  $\lambda_{\text{max}} \approx 0.55 \mu\text{m}$  (Whittet 2003).

The linear dichroism is characterized by a polarization cross section at wavelength  $\lambda$  per H nucleon

$$\sigma_{\text{pol}}^{(\text{obs})}(\lambda) \equiv \frac{\Delta\tau}{N_{\text{H}}} = \frac{1}{N_{\text{H}}} \text{arctanh}[p(\lambda)], \quad (3)$$

which, for  $p \ll 1$ , can be approximated as

$$\sigma_{\text{pol}}^{(\text{obs})}(\lambda) \approx \frac{p(\lambda)}{N_{\text{H}}}. \quad (4)$$

The strength of the polarization is characterized by the polarization per unit extinction  $p_{\text{max}}/A(\lambda_{\text{max}})$ , where  $p_{\text{max}} = p(\lambda_{\text{max}})$ . On some sightlines the polarization per unit extinction is as large as  $p_{\text{max}}/A(\lambda_{\text{max}}) \approx 0.03/\text{mag}$  (Whittet 2003). Smaller values of  $p_{\text{max}}/A(\lambda_{\text{max}})$  are presumed to arise where the local magnetic field is not orthogonal to the sightline, where the magnetic field direction varies along the line-of-sight, or where the processes responsible for grain alignment are for some reason less effective. A successful grain model must be able to account for the largest observed values, i.e.,  $p_{\text{max}}/A(\lambda_{\text{max}}) \approx 0.03/\text{mag}$ .

Various approaches have been taken to describing the wavelength dependence of interstellar polarization [see, e.g., Martin et al. (1999)]. Following Draine & Allaf-Akbari (2006), we take it to be given by the empirical “Serkowski law” (Serkowski 1973)

$$p(\lambda) \approx p_{\text{max}} \exp \left[ -K \left( \ln \frac{\lambda}{\lambda_{\text{max}}} \right)^2 \right] \quad (5)$$

for  $0.15 < \lambda < 1.39 \mu\text{m}$ , with  $\lambda_{\text{max}} = 0.55 \mu\text{m}$  and  $K = 0.92$ . For  $1.39 < \lambda < 5 \mu\text{m}$ , we assume the power-law dependence  $p(\lambda) \propto \lambda^{-1.7}$ , consistent with the observations by Martin et al. (1992).

## 3. DUST MODELS

As in previous studies (Weingartner & Draine 2001; Draine & Allaf-Akbari 2006), we model the dust as a mixture of carbonaceous particles (including PAHs) and amorphous silicate grains. Models of the infrared emission from interstellar dust (Li & Draine 2001; Draine & Li 2007) require a population of very small PAH particles, containing C/H  $\approx 55$  ppm, or about 22% of all of the C atoms if the C abundance in the ISM is equal to the the current best estimate for the solar abundance  $(\text{C}/\text{H})_\odot = (247 \pm 28) \text{ ppm}$  (Asplund et al. 2005). We assume the PAHs to have the absorption cross sections given by Draine & Li (2007), with a strong absorption feature at  $2175 \text{ \AA}$ , and to contribute  $\sigma_{\text{ext}}(\text{PAH}, \lambda)$  to the overall extinction. The PAH population is expected to be randomly-oriented (Lazarian & Draine 1999), and therefore is assumed to contribute no polarization. This is consistent with the observed weakness or absence of polarization in the aforementioned  $2175 \text{ \AA}$  feature (Clayton et al. 1992; Wolff et al. 1997).

In addition to the PAHs, the model includes populations of larger silicate particles and carbonaceous

grains. The size distribution of these particles is a priori unknown, as is the degree of alignment. To determine these quantities, we will follow the approach pioneered by Kim & Martin (1995), seeking to find a model grain size distribution and size-dependent degree of alignment that can simultaneously reproduce both the wavelength-dependent extinction cross section  $\sigma_{\text{ext}}(\lambda)$  and the wavelength-dependent polarization  $\sigma_{\text{pol}}(\lambda)$ .

In our models, the dust grains will be assumed to be oblate spheroids, with semimajor axis  $a$  along the symmetry axis  $\hat{\mathbf{a}}$ , and  $b > a$  perpendicular to this axis. For a given axial ratio  $b/a$ , we characterize the grain size by the effective radius  $a_{\text{eff}} \equiv (ab^2)^{1/3}$ , which corresponds to the radius of an equal-volume sphere.

#### 4. OPTICAL CROSS SECTIONS

For a nonspherical grain of solid volume  $V$ , we define the extinction efficiency factor

$$Q_{\text{ext}} \equiv \frac{C_{\text{ext}}}{\pi a_{\text{eff}}^2}, \quad (6)$$

where  $C_{\text{ext}}$  is the extinction cross section, and  $a_{\text{eff}}$  the radius of an equal-volume sphere, i.e.,  $(3V/4\pi)^{1/3}$ . The extinction cross sections for polarized light are calculated for oblate spheroids using the “extended boundary condition method” (EBCM) introduced by Waterman (1971) and developed by Mishchenko & Travis (1994) and Wiegand et al. (1997). We use the open-source code `ampld.lp.f` made available by Mishchenko (2000). EBCM codes encounter numerical difficulties when the target becomes large compared to the wavelength. For the silicate oblate spheroids ( $b/a > 1$ ), we find that `ampld.lp.f` sometimes fails for  $b/\lambda > 3.885$ . Thus, for  $b/\lambda > 3.885$ , and for both  $b/a = 1.4$  and  $b/a = 1.6$  (values we will focus on from now on), we take

$$Q_{\text{ext}}[b/\lambda, b/a, \lambda] \approx Q_{\text{ext}}[3.885, b/a, \lambda] \quad (7)$$

for silicates. The EBCM assumes an isotropic dielectric function, but graphite is a highly anisotropic material. The eigenvalues of the graphite dielectric tensor are  $(\epsilon_{\parallel}, \epsilon_{\perp}, \epsilon_{\perp})$ . In order to estimate  $Q_{\text{ext}}$  and  $Q_{\text{pol}}$  for spheroids composed of graphite, we use the so-called “1/3-2/3 approximation”: we assume that 1/3 of the spheroids have an isotropic dielectric function  $\epsilon = \epsilon_{\parallel}$ , while 2/3 of them have  $\epsilon = \epsilon_{\perp}$ . This gives the correct cross sections in the “electric dipole limit”  $a_{\text{eff}} \ll \lambda$ , and Draine & Malhotra (1993) used the discrete dipole approximation to show that the 1/3-2/3 approximation is reasonably accurate even for finite grain size. The actual composition of the carbonaceous grains is unknown. Based on the profile of the 3.4  $\mu\text{m}$  C-H stretching mode, Pendleton & Allamandola (2002) estimate that about 85% of the carbon is in aromatic structures. We do not expect interstellar grains to be single-crystal graphite, but it is hoped that the approach adopted here will provide cross sections that will approximate the carbonaceous material present in the interstellar medium.

The dielectric function for graphite is somewhat more extreme in the ultraviolet than that for silicate. For the graphite oblate spheroids, we find that `ampld.lp.f` sometimes fails for  $b/\lambda > 2.023$ . Thus, for graphite grains with  $b/\lambda > 2.023$ , we take

$$Q_{\text{ext}}[b/\lambda, b/a, \lambda] \approx Q_{\text{ext}}[2.023, b/a, \lambda]. \quad (8)$$

The top panel of Figure 1 shows  $Q_{\text{ext}}$  as a function of  $2\pi b/\lambda$  at four selected wavelengths for randomly-oriented<sup>1</sup> silicate spheroids with  $b/a = 1.4$  and  $b/a = 1.6$ . In the limit  $b/a \rightarrow \infty$ , we expect  $Q_{\text{ext}} \pi a_{\text{eff}}^2$  to approach twice the geometric cross section, with 50% of the total extinction produced by rays that impinge on the grain, and 50% contributed by small angle scattering resulting from diffraction [see, e.g., the discussion of the “extinction paradox” in Bohren & Huffman (1983)]. If (1/3, 1/3, 1/3) of the spheroids have symmetry axis ( $\hat{\mathbf{a}} \parallel \hat{\mathbf{x}}, \hat{\mathbf{a}} \parallel \hat{\mathbf{y}}, \hat{\mathbf{a}} \parallel \hat{\mathbf{z}}$ ), the extinction efficiency factor for light propagating in the  $\hat{\mathbf{x}}, \hat{\mathbf{y}}$ , or  $\hat{\mathbf{z}}$  directions is such that

$$Q_{\text{ext}}(b/\lambda \rightarrow \infty) = \frac{2}{3} \left[ (b/a)^{2/3} + 2(a/b)^{1/3} \right]. \quad (9)$$

The horizontal dashed line shows this limiting value; we see that the calculated cross sections appear to be converging to this limit. Our assumption summarized by equation (7) will overestimate  $Q_{\text{ext}}$  slightly. However, for realistic size distributions, the extinction at  $\lambda > 0.1 \mu\text{m}$  is generally dominated by grains with  $b/\lambda \lesssim 1$ .

The bottom panel of Figure 1 is the same as the top panel, but for graphite spheroids. Note that while  $Q_{\text{ext}}$  for the silicate spheroids reaches values as large as 4.7 (for  $\lambda = 0.215 \text{ \AA}$  in the top panel), the carbon grains reach only  $Q_{\text{ext}} \approx 3.1$  for  $b/a = 1.4$ , and  $Q_{\text{ext}} \approx 2.8$  for  $b/a = 1.6$ ; the refractive index matters! We also see that the extinction approaches twice the geometric cross section for  $b/\lambda \gtrsim 2$ , so we may use equation (8) to estimate  $Q_{\text{ext}}$  for large values of  $b/\lambda$ .

Finally, Figure 2 shows extinction cross sections as a function of wavelength for silicate and carbon spheroids of selected values of the effective radius  $a_{\text{eff}}$ .

#### 5. PICKET-FENCE ALIGNMENT

The process of interstellar grain alignment [see, e.g., Roberge (2004)] leads to the short axis of grains (the axis with the largest moment of inertia) tending to align with the magnetic field direction. For oblate spheroids, the symmetry axis  $\hat{\mathbf{a}}$  therefore aligns with the magnetic field, and maximum polarization of starlight occurs for sightlines perpendicular to the magnetic field direction.

We adopt a coordinate system with the line-of-sight in the  $\hat{\mathbf{z}}$  direction, and the magnetic field in the  $\hat{\mathbf{x}}$  direction. For simplicity, we will assume “picket-fence” alignment, i.e., that a fraction  $(1+2f)/3$  of the oblate spheroids are oriented with the symmetry axis  $\hat{\mathbf{a}}$  in the  $\hat{\mathbf{x}}$  direction, a fraction  $(1-f)/3$  with  $\hat{\mathbf{a}} \parallel \hat{\mathbf{y}}$ , and a fraction  $(1-f)/3$  with  $\hat{\mathbf{a}} \parallel \hat{\mathbf{z}}$ . Thus,  $f = 0$  corresponds to random orientation (1/3 of the grains in each orientation), and  $f = 1$  to perfect alignment (all of the grains with  $\hat{\mathbf{a}} \parallel \hat{\mathbf{x}}$ ).

“Picket-fence” alignment is not physically realistic. Interstellar grains will have a continuous distribution of orientations, and a grain with angular momentum that is not aligned with  $\mathbf{B}$  will precess around  $\mathbf{B}$ . The advantage of assuming picket-fence alignment is that for each grain size and wavelength, the extinction cross section needs to be calculated for only 3 grain orientations. We expect that picket-fence alignment with alignment fraction  $f$  will closely reproduce the polarization produced

<sup>1</sup> Random orientation is approximated by averaging over the three independent orientations of spheroids in the “picket-fence” approximation described in §5.

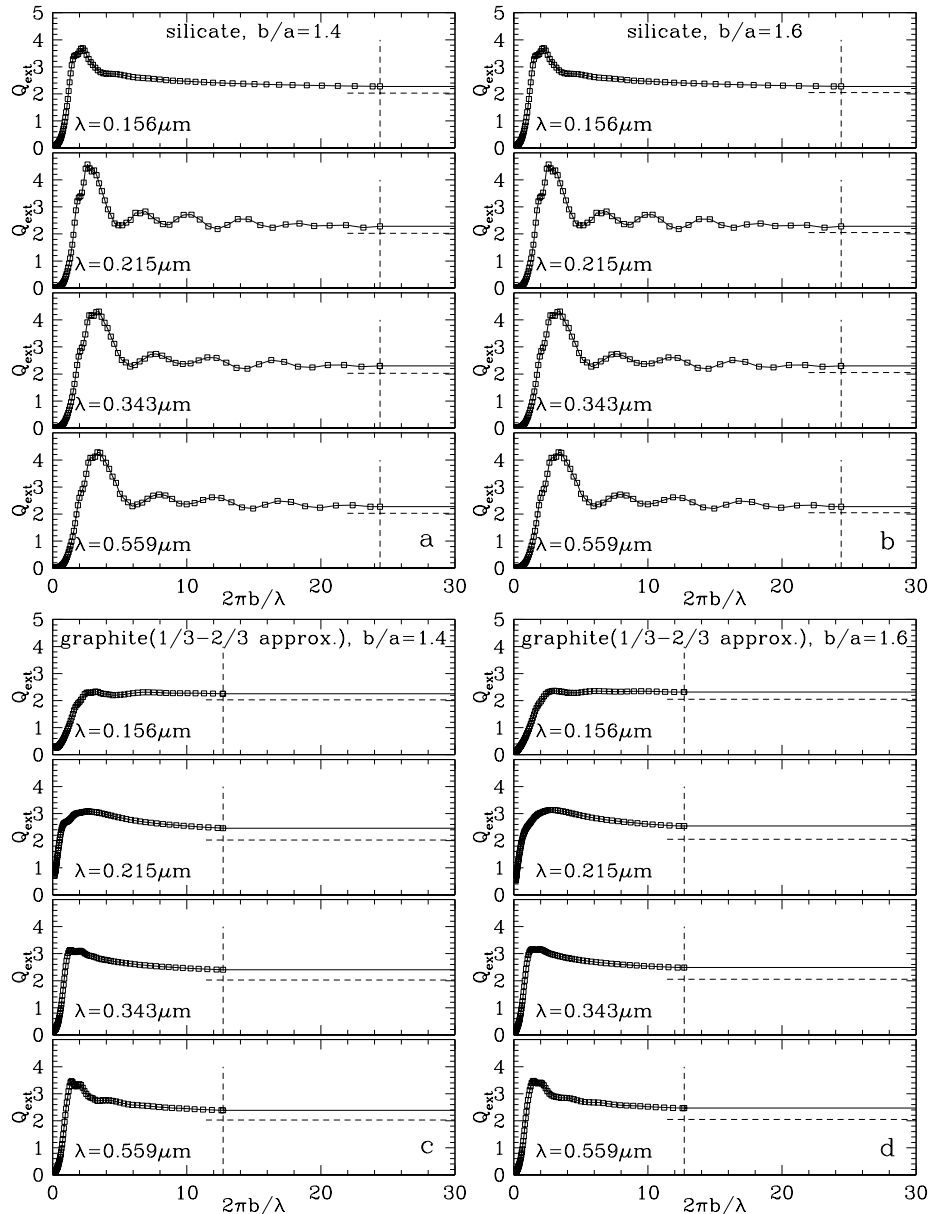


FIG. 1.—  $Q_{\text{ext}}(b/\lambda, b/a, \lambda)$  vs.  $2\pi b/\lambda$  at four wavelengths for randomly-oriented silicate (*top*) and graphite (*bottom*) spheroids with axial ratios  $b/a$  of 1.4 and 1.6. The vertical dashed lines show the maximum value of  $2\pi b/\lambda$  allowed by the EBCM calculations with the silicate dielectric function. Horizontal dashed lines indicate  $Q_{\text{ext}}(b/\lambda \rightarrow \infty, b/a, \lambda)$  in each case.

by grains with a continuous distribution of alignments provided  $f = (3/2) [\langle (\hat{\mathbf{a}} \cdot \hat{\mathbf{x}})^2 \rangle - (1/3)]$ .

Let  $C_{\text{ext},j}(m, a_{\text{eff}}, b/a, \lambda)$  be the extinction cross section at wavelength  $\lambda$  for a spheroid of material  $m$ , with effective radius  $a_{\text{eff}}$  and axial ratio  $b/a$ , where  $j$  refers to the orientation of the grain relative to incident polarized light. We discretize the size range into  $N$  size bins  $a_{\text{eff},i}$  (with  $i \in [1, N]$ ), uniformly spaced in  $\log(a_{\text{eff},i})$ , with  $n_{\text{sil},i}$  and  $n_{\text{car},i}$  the numbers of silicate and carbonaceous grains per H nucleon, and  $f_i$  the fractional alignment

of grains of size  $a_{\text{eff},i}$ . The process of interstellar grain alignment remains uncertain, and it is possible that the alignment function  $f$  might depend on grain composition as well as on grain size. In this paper, we will assume that  $f_i$  depends only on grain size, not on the material.

The “average” extinction curve we will fit to is an average over sightlines making various angles to the magnetic field direction, so it is appropriate to compare the observed extinction with the extinction calculated for randomly-oriented spheroids.

We define the dimensionless efficiency factor for extinction by randomly-oriented grains through

$$Q_{\text{ext}}\left(m, \frac{a_{\text{eff}}}{\lambda}, \frac{b}{a}\right) \equiv \frac{1}{\pi a_{\text{eff}}^2} \frac{1}{3} \sum_{j=1}^3 C_{\text{ext},j}\left(m, a_{\text{eff}}, \frac{b}{a}, \lambda\right). \quad (10)$$

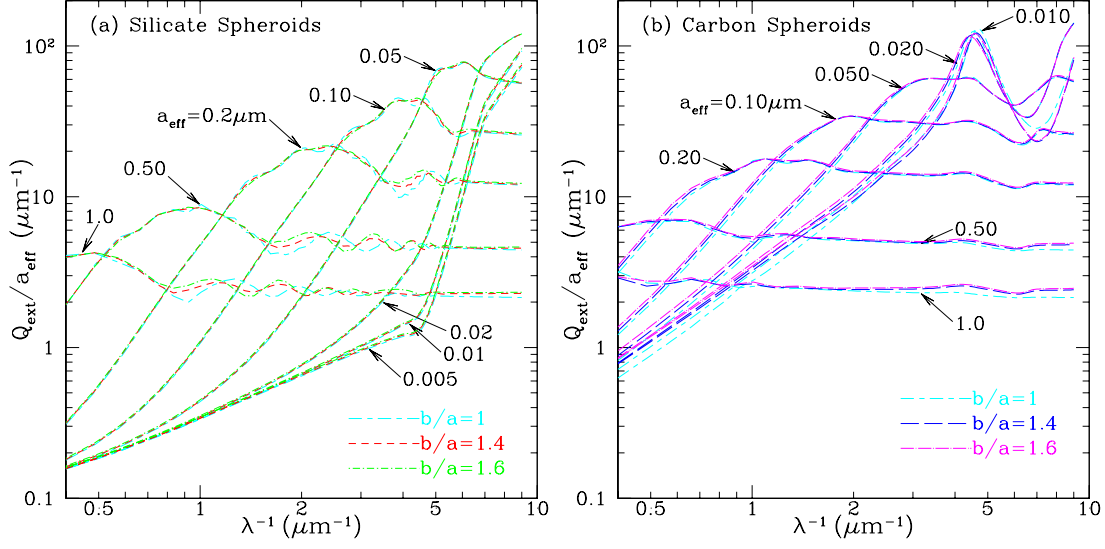


FIG. 2.— Extinction cross sections  $Q_{\text{ext}}(a_{\text{eff}}, b/a, \lambda)/a_{\text{eff}}$  vs. inverse wavelength  $1/\lambda$  for (left) silicate, and (right) graphite spheres and spheroids with axial ratios of  $b/a = 1.4$  and  $b/a = 1.6$ . Curves are labeled by  $a_{\text{eff}}$  (in  $\mu\text{m}$ ).

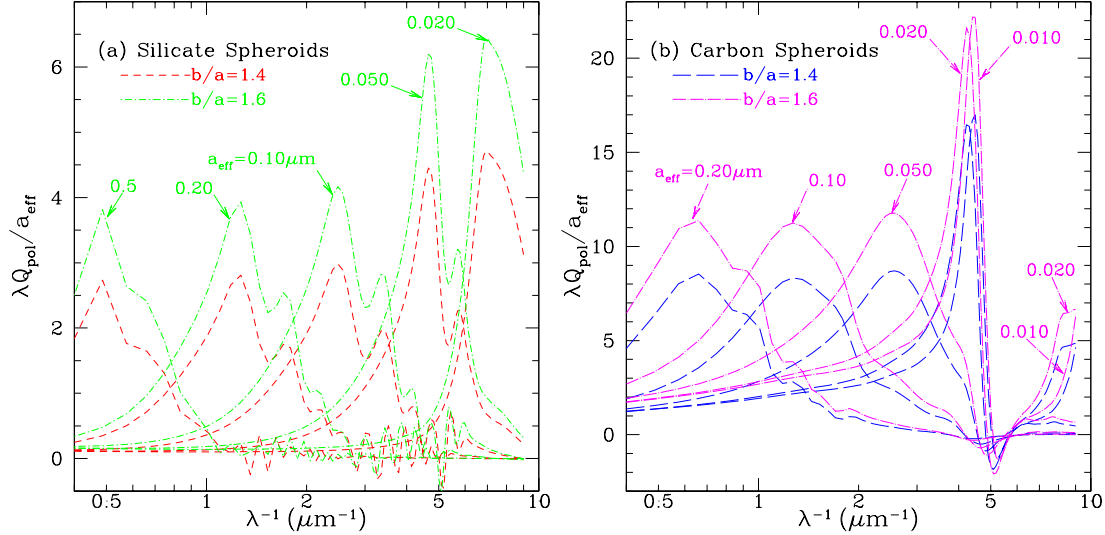


FIG. 3.—  $\lambda Q_{\text{pol}}/a_{\text{eff}}$  vs. inverse wavelength for (left) silicate spheroids, and (right) graphite spheroids with axial ratios  $b/a = 1.4$  and  $b/a = 1.6$ . Curves are labeled by  $a_{\text{eff}}$  (in  $\mu\text{m}$ ). The pronounced drop in  $Q_{\text{pol}}$  for graphite grains as  $\lambda$  increases from 0.20  $\mu\text{m}$  to 0.22  $\mu\text{m}$  is a result of the wavelength dependence of the dielectric function  $\epsilon_{\perp}$  (see text).

The index  $j$  runs from 1 to 3 as we require three orientations for picket-fence alignment with oblate spheroids:

$$\begin{aligned} j=1 & \text{ for } \mathbf{k} \perp \hat{\mathbf{a}} \text{ and } \mathbf{E} \parallel \hat{\mathbf{a}}, \\ j=2 & \text{ for } \mathbf{k} \perp \hat{\mathbf{a}} \text{ and } \mathbf{E} \perp \hat{\mathbf{a}}, \\ j=3 & \text{ for } \mathbf{k} \parallel \hat{\mathbf{a}} \text{ and } \mathbf{E} \perp \hat{\mathbf{a}}, \end{aligned} \quad (11)$$

where  $\mathbf{k}$  is the incident wavevector. We also define an efficiency factor for polarization by perfectly-aligned grains:

$$Q_{\text{pol}}\left(m, \frac{a_{\text{eff}}}{\lambda}, \frac{b}{a}\right) \equiv \frac{1}{\pi a_{\text{eff}}^2} \frac{1}{2} \left[ C_{\text{ext},2}\left(m, a_{\text{eff}}, \frac{b}{a}, \lambda\right) - C_{\text{ext},1}\left(m, a_{\text{eff}}, \frac{b}{a}, \lambda\right) \right]. \quad (12)$$

Figure 3 shows the polarization efficiency factors  $Q_{\text{pol}}$  as a function of wavelength  $\lambda$  for selected sizes of silicate and carbon spheroids. Note that  $Q_{\text{pol}}$  tends to peak near  $2\pi a_{\text{eff}}/\lambda \approx 1.6$  for the silicate spheroids, whereas it peaks near 0.8 for the carbon spheroids. Small carbon spheroids show a strong peak in  $Q_{\text{pol}}$  near  $\lambda \approx 0.23 \mu\text{m}$ ; this is a result of the strong peak in  $\text{Im}(\epsilon_{\perp})$  due to  $\pi \rightarrow \pi^*$  electronic transitions near this frequency.

The model we consider here involves a mixture of silicate and carbon (including PAHs) dust grains. In such a case, the extinction cross section per H nucleon is given by

$$\sigma_{\text{ext}}(\lambda) = \sigma_{\text{ext}}(\text{PAH}, \lambda) + \sum_m \sum_{i=1}^N n_{m,i} \pi a_{\text{eff},i}^2 Q_{\text{ext}}\left[m, \frac{a_{\text{eff},i}}{\lambda}, \left(\frac{b}{a}\right)_m\right], \quad (13)$$

where we sum over materials  $m = \{\text{sil}, \text{car}\}$  and over grain size  $a_{\text{eff},i}$ , with  $n_{m,i}$  the number of grains of composition  $m$  and size  $a_{\text{eff},i}$  per H nucleon. The polarization cross section for the model is

$$\sigma_{\text{pol}}(\lambda) = \sum_m \sum_{i=1}^N f_i n_{m,i} \pi a_{\text{eff},i}^2 Q_{\text{pol}} \left[ m, \frac{a_{\text{eff},i}}{\lambda}, \left( \frac{b}{a} \right)_m \right]. \quad (14)$$

A priori, we do not know the grain shape, except that the grains must be sufficiently nonspherical to be able to reproduce the observed polarization of starlight. We will proceed using trial grain shapes, and will see whether we are able to reproduce the polarization with a size-dependent alignment fraction  $f(a) \leq 1$ .

For a given model (with assumed axial ratio  $(b/a)_m$  for material  $m$ ), we use the technique described in §4 to obtain the cross sections  $C_{\text{ext},j}[m, a_{\text{eff},i}, (b/a)_m, \lambda]$ , and then seek the abundances  $n_{i,m}$  and alignment function  $f_i$  that minimize a positive-definite penalty function

$$P = \sum_{\ell} (\Psi_{\ell})^2, \quad (15)$$

where the  $\Psi_{\ell}$ 's are measures of deviation from an ideal fit to the data. We use the penalty function described by Draine & Allaf-Akbari (2006), which includes a contribution proportional to the square of the deviation of the model extinction curve from the observed extinction curve, and a contribution proportional to the square of the deviation of the model polarization curve from the observed polarization curve, as well as terms that measure the non-smoothness of the size distributions  $n_{\text{sil},i}$  and  $n_{\text{car},i}$ , and of the alignment function  $f_i$ . The degree to which the amount of material in the model grains deviates from the amount of material ‘‘depleted’’ from the gas, as inferred from observations of ultraviolet absorption lines (Jenkins 2004), also contributes to the penalty  $P$ .

TABLE 1  
MODELS

Model number	$b/a$ (silicate)	$b/a$ (carbon)	$V_{\text{sil}}$ ( $10^{-27} \text{cm}^3/\text{H}$ )	$V_{\text{car}}^{\text{a}}$ ( $10^{-27} \text{cm}^3/\text{H}$ )
0	1.0	1.0	3.00	1.91
1	1.4	1.0	3.81	1.93
2	1.4	1.4	3.34	1.89
3	1.6	1.0	3.18	1.92
4	1.6	1.6	3.20	1.89
‘‘Observed’’			2.50	1.00

<sup>a</sup>Including C/H = 55 ppm in PAH material, with assumed carbon density 2.24 g/cm<sup>3</sup>.

## 6. SIZE DISTRIBUTIONS AND ALIGNMENT FUNCTIONS

Polarization in the 9.7  $\mu\text{m}$  silicate feature is routinely observed (Smith et al. 2000), and therefore it is clear that the silicate grains must be nonspherical. As a result, all of our models (1 – 4) include spheroidal silicate grains, with axial ratios  $b/a = 1.4$  or  $b/a = 1.6$ . Because there is no observational evidence of polarization produced by carbonaceous grains, we will consider two possibilities, namely, that the carbonaceous grains are spherical, or just as nonspherical (and aligned) as the silicates.

We study four models involving nonspherical grains. Model 1 has spheroidal silicate grains with  $b/a = 1.4$ , and spherical carbon grains. Model 2 assumes both silicate and carbon grains to be spheroids with  $b/a = 1.4$ . Model 3 considers silicate spheroids with a more extreme axial ratio,  $b/a = 1.6$ , but with spherical carbon grains. Finally, our fourth model assumes both silicate and carbon grains to be spheroids with  $b/a = 1.6$ .

We obtained the best-fit grain abundances  $n_{i,\text{car}}$  and  $n_{i,\text{sil}}$ , and degree of alignment  $f_i$ , for these four distinct models using the Levenberg-Marquardt algorithm to minimize the penalty function  $P$  discussed in §5.

Figure 4 shows the ‘‘observed extinction’’ that we seek to reproduce, together with the extinction obtained for each model. For comparison purposes, we also carried

out a fit to the extinction using spherical silicate and carbon grains (model 0), with no consideration of polarization. Note that all models are more-or-less equally good at reproducing the observed extinction. All of the models tend to underpredict the extinction for  $\lambda \gtrsim 1.2 \mu\text{m}$ , suggesting that perhaps our adopted composition is insufficiently absorptive at  $\lambda \approx 2 \mu\text{m}$ . It should be kept in mind, however, that the ‘‘observed’’ extinction is somewhat uncertain at the longer wavelengths, owing to the increasing difficulty in determining the extinction per H nucleon when the H column density cannot be determined directly using Lyman- $\alpha$  absorption measurements.<sup>2</sup> Nishiyama et al. (2006) find  $A_{\lambda} \propto \lambda^{-1.99}$  for  $1.25 \leq \lambda \leq 2.2 \mu\text{m}$ , steeper than the ‘‘observed’’ extinction used here, and closer to the behavior in our models. The volumes of silicate and carbonaceous materials required by each model is given in Table 1.

### *Elemental Abundances*

The most recent estimates of solar abundances indicate that Mg/H = 38 ppm (Grevesse & Sauval 1998), and Si/H = 32 ppm and Fe/H = 29 ppm (Asplund 2000).

<sup>2</sup> To accurately measure the weaker extinction in the infrared, larger dust columns are needed, but the ultraviolet extinction is then so strong that Lyman- $\alpha$  measurements become infeasible.

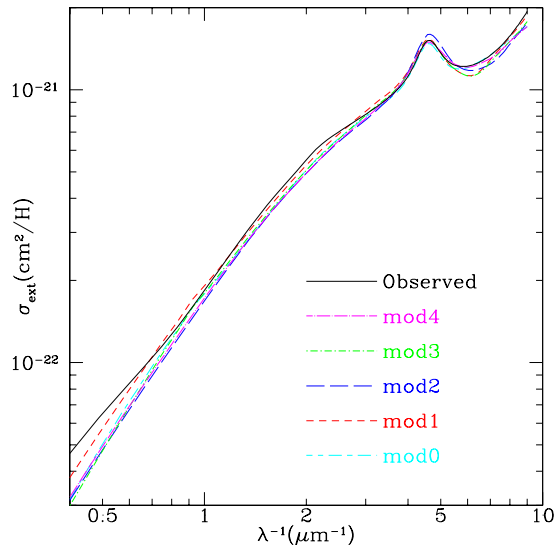


FIG. 4.— Extinction per H nucleon as a function of inverse wavelength for models 0, 1, 2, 3, and 4 (see Table 1). The solid line corresponds to the “observed” extinction (as defined in § 5), which appears to be well fit by all five of our models at all wavelengths of interest.

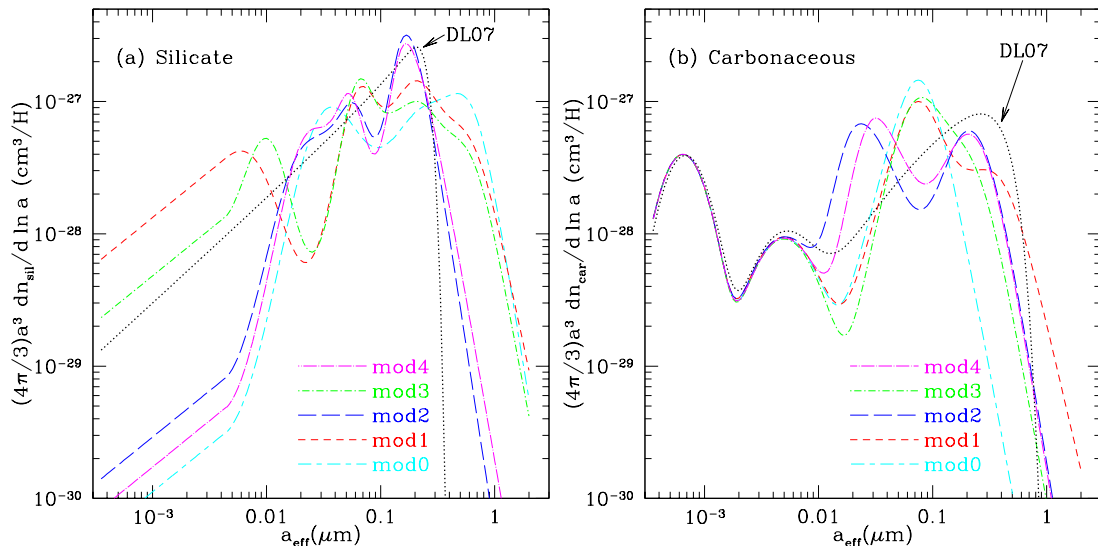


FIG. 5.— Mass distribution for (left) silicate and (right) graphite spheres and spheroids. Results are shown for models 0 through 4. The curves labeled “DL07” show the size distributions of Weingartner & Draine (2001), as modified by Draine & Li (2007).

If all of the Si is consumed, we could form silicate material with the olivine-like composition  $\text{Mg}_{1.1}\text{Fe}_{0.9}\text{SiO}_4$ . The density of Si atoms in fayalite ( $\text{Fe}_2\text{SiO}_4$ ) is about  $1.3 \times 10^{22} \text{ cm}^{-3}$ . With this density of Si,  $\text{Mg}_{1.1}\text{Fe}_{0.9}\text{SiO}_4$  would have density  $\rho \approx 3.7 \text{ g/cm}^3$ , and the solar abundance of Si could produce  $V = 2.5 \times 10^{-27} \text{ cm}^3/\text{H}$  of silicate material. Thus, we see that the silicate volumes in Table 1 exceed what appears to be allowed by current estimated solar abundances by 20% to 50%.

For a carbon density of  $2.2 \text{ g/cm}^3$ , the carbon volume in model 0 corresponds to  $\text{C}/\text{H} = 210 \text{ ppm}$ . On the well-studied sightline toward  $\zeta \text{ Oph}$ , the gas-phase carbon abundance is about 135 ppm (Cardelli et al. 1993). Adding this to our estimate for the carbon in dust grains would give an interstellar  $\text{C}/\text{H} = 345 \text{ ppm}$ , 40% greater than the most recent estimate of the solar abundance  $(\text{C}/\text{H})_{\odot} = 245 \pm 30 \text{ ppm}$  (Asplund et al. 2005).

The amount of grain material called for in these fits is

cause for concern – our models tend to require about 40% more silicates and carbon than appears to be available if interstellar abundances are the same as solar abundances. However, interstellar abundances of C, Mg, Si, and Fe may exceed the abundances of these elements in the Sun. Furthermore, solar abundances may have been underestimated. For example, it has recently been argued that the oxygen abundance in the solar photosphere has been underestimated by a factor of about 2 (Landi et al. 2007; Centeno & Socas-Navarro 2008).

Figure 5 shows the size distributions for the silicate grains and the carbon grains for our five dust models. Two classes of models are clearly visible. The models where only the silicate grains are aligned (models 1 and 3) have broad distributions for the silicates, while the carbonaceous grains have a pronounced peak near  $0.08 \mu\text{m}$ . On the other hand, in models where both silicate and

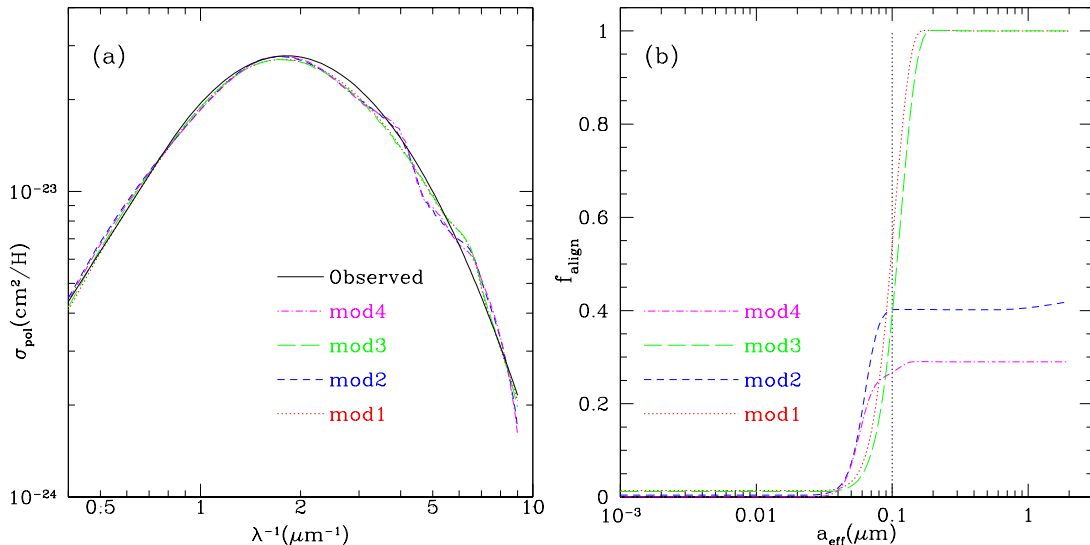


FIG. 6.— (Left) Polarization cross section per H nucleon vs. inverse wavelength from observations (solid curve) and for models 1, 2, 3, and 4 (see Table 1). (Right) Fractional alignment  $f$  vs.  $a_{\text{eff}}$  for these four grain models. The vertical dotted line shows  $a_{\text{eff}} = 0.1 \mu\text{m}$ .

carbonaceous grains are aligned (models 2 and 4), the silicate size distributions have a dominant peak near  $0.15 \mu\text{m}$ , while the carbonaceous grains have pronounced peaks near  $0.03 \mu\text{m}$  and  $0.25 \mu\text{m}$ . Despite these differences, all of the models 1 through 4 produce polarization that is in reasonable agreement with the observations, as can be seen in Figure 6, but this is achieved with quite different alignment functions  $f(a)$ , also shown in Figure 6. The models with spherical carbon grains (models 1 and 3) have alignment functions that rise rapidly from near-zero to near-unity at  $a \approx 0.1 \mu\text{m}$ . When non-

spherical carbon grains are included, however, the large polarization cross sections for the carbon grains mean that the required polarization can be achieved without complete alignment of the  $a \gtrsim 0.15 \mu\text{m}$  grains. For model 2 ( $b/a = 1.4$ ), the alignment for  $a_{\text{eff}} \gtrsim 0.1 \mu\text{m}$  is  $f \approx 0.4$ ; when  $b/a$  is increased to 1.6, the alignment of the larger grains drops to about 0.3. Note that these alignment functions reproduce the highest observed values of  $P_{\text{max}}/A_V$ . It is possible that, in some regions, the dust grains have lower degrees of alignment.

## 7. FAR-INFRA-RED CROSS SECTIONS AND EMISSIVITIES

At wavelengths  $\lambda \gg a$  (the ‘‘Rayleigh limit’’), the absorption cross section of a grain depends only on the orientation of the oscillating electric field relative to the grain shape, and not on the direction of the oscillating magnetic field (i.e.,  $C_{\text{abs},3} = C_{\text{abs},2}$ ). For a spheroid, the absorption cross section is then

$$C_{\text{abs}} = C_{\text{abs},1} \cos^2 \zeta + C_{\text{abs},2} \sin^2 \zeta, \quad (16)$$

where  $\zeta$  is the angle between the electric field  $\mathbf{E}$  and the symmetry axis  $\hat{\mathbf{a}}$ . Randomly-oriented spheroids have  $\langle \cos^2 \zeta \rangle = 1/3$ , which leads to the ‘‘average’’ absorption cross section

$$\langle C_{\text{abs}} \rangle = \frac{1}{3}(C_{\text{abs},1} + 2C_{\text{abs},2}). \quad (17)$$

Let  $\theta_0$  be the angle between the direction of the magnetic field,  $\hat{\mathbf{x}}$ , and the direction of propagation. We denote quantities for radiation with  $\mathbf{E}$  parallel (respectively, perpendicular) to the  $(\mathbf{k}, \hat{\mathbf{x}})$  plane with the label  $\parallel$  (respectively,  $\perp$ ). If a fraction  $f$  of the grains is perfectly aligned, and a fraction  $(1 - f)$  is randomly-oriented,

$$\langle \cos^2 \zeta_{\parallel} \rangle = \frac{1-f}{3} + f \sin^2 \theta_0, \quad (18)$$

$$\langle \cos^2 \zeta_{\perp} \rangle = \frac{1-f}{3}. \quad (19)$$

The polarization-averaged absorption cross section is then given by

$$C_{\text{abs}} \equiv \frac{1}{2}(C_{\text{abs}}^{\perp} + C_{\text{abs}}^{\parallel}) = \frac{1}{2} \left\{ C_{\text{abs},1} \left[ \frac{2}{3} - f \left( \cos^2 \theta_0 - \frac{1}{3} \right) \right] + C_{\text{abs},2} \left[ \frac{4}{3} + f \left( \cos^2 \theta_0 - \frac{1}{3} \right) \right] \right\}, \quad (20)$$

whereas the cross section for polarized emission is defined as

$$C_{\text{pol}} \equiv \frac{1}{2}(C_{\text{abs}}^{\perp} - C_{\text{abs}}^{\parallel}) = \frac{1}{2} f (C_{\text{abs},2} - C_{\text{abs},1}) \sin^2 \theta_0. \quad (21)$$



Therefore, for a mixture of partially-aligned grains, the total and polarized emissivities are

$$\begin{aligned} \frac{1}{N_H} I_\lambda(\theta_0) &= \frac{1}{3} \sum_m \int da_{\text{eff}} \frac{dn_m}{da_{\text{eff}}} (2C_{\text{abs},2} + C_{\text{abs},1}) \langle B_\lambda \rangle_{m,a_{\text{eff}}} \\ &\quad + \frac{1}{2} \left( \cos^2 \theta_0 - \frac{1}{3} \right) \sum_m \int da_{\text{eff}} \frac{dn_m}{da_{\text{eff}}} f(a_{\text{eff}}) (C_{\text{abs},2} - C_{\text{abs},1}) \langle B_\lambda \rangle_{m,a_{\text{eff}}}, \end{aligned} \quad (22)$$

$$\frac{1}{N_H} I_{\lambda,\text{pol}}(\theta_0) = \frac{1}{2} \sin^2 \theta_0 \sum_m \int da_{\text{eff}} \frac{dn_m}{da_{\text{eff}}} f(a_{\text{eff}}) (C_{\text{abs},2} - C_{\text{abs},1}) \langle B_\lambda \rangle_{m,a_{\text{eff}}}, \quad (23)$$

where

$$\langle B_\lambda \rangle_{m,a_{\text{eff}}} \equiv \int dT \frac{dP(a_{\text{eff}}, m, U)}{dT} B_\lambda(T), \quad (24)$$

$dP(a_{\text{eff}}, m, U)/dT$  is the temperature distribution for grains of type  $m$  and size  $a_{\text{eff}}$  in a radiation field of intensity  $U$ , and  $B_\lambda(T)$  the Planck function. We use the temperature distributions computed by Draine & Li (2007) for spherical grains. For the spheroidal components of our models, we correct these distributions to account for the non-sphericity of the grains by requiring that the power they absorb equals the power they re-radiate. The correction is very small.

## 8. RESULTS AND DISCUSSION

Figure 7 shows the emission spectra calculated for each of the five grain models listed in Table 1 when illuminated by the standard interstellar radiation field for the solar neighborhood. Also shown is the emission spectrum calculated for the grain model of Draine & Li (2007). The emission  $\langle I_\lambda \rangle$  is calculated using the cross section  $\langle C_{\text{abs}} \rangle$  from equation (17), appropriate for randomly-oriented dust. These spectra of the thermal emission do not include rotational emission from spinning dust, which appears to dominate for  $\lambda \gtrsim 4000 \mu\text{m}$  ( $\nu \lesssim 75 \text{ GHz}$ ) (Draine & Lazarian 1998; Finkbeiner 2004).

The emission spectra for all six models are relatively similar. In each case,  $\lambda \langle I_\lambda \rangle$  peaks near  $130 \mu\text{m}$ , with an amplitude within 20% of the Draine & Li (2007) (thereafter, DL07) model. Moreover, all models agree extremely well for wavelengths below about  $20 \mu\text{m}$ , where the signal is entirely dominated by PAH features.

However, there are some noticeable differences, especially in the ratio of the  $130 \mu\text{m}$  to the  $24 \mu\text{m}$  emissions. Although these ratios are within 15% of each other for model 0 and the DL07 model, models involving spheroidal grains lead to smaller values of this ratio, typically by a factor of 1.5. This difference arises mostly from variations in the size distributions between models, with differences in grain shape also having a small effect on the average emission spectrum. All other differences are fairly modest (usually at the 10% to 20% level), and generally smaller than the actual uncertainties in the appropriate dielectric functions.

The fact that all of these spectra are in good agreement overall, but with significant well localized differences, opens a very interesting window through which one can hope to strongly constrain dust models with observations of the total dust emission at just a couple of wavelengths. We have not attempted this exercise here.

Figure 8 shows the polarized emission spectra calculated for models 1 through 4, as well as the corresponding degrees of polarization (in %), for lines of sight perpendicular to the direction of the local magnetic field, and the dust exhibiting the highest degrees of alignment found in the diffuse interstellar medium.

Contrary to the total emission spectra shown on Figure 7, the polarized emission spectra clearly reflects the fact that we consider two classes of models. The spectra of polarized emission for models 2 and 4, with spheroidal silicate and carbonaceous grains, are indeed remarkably similar, but quite different from those for models 1 and 3, with silicate spheroids and carbonaceous spheres. This translates into interestingly different predictions for the expected degree of polarization for emission by interstellar dust, as can be seen in the right panel of Figure 8.

Although all models predict virtually no polarization below  $40 \mu\text{m}$  (as small grains and PAHs are not aligned), the wavelength dependence of the degree of polarization for  $\lambda \gtrsim 40 \mu\text{m}$  is quite model-dependent. Models with both silicate and carbonaceous spheroidal grains lead to the degree of polarization sharply increasing between about  $40 \mu\text{m}$  and  $600 \mu\text{m}$ , after which it reaches a plateau. However, the degree of polarization for models in which only the silicate grains are spheroids increases steadily with increasing wavelength, without converging to an upper limit. As a result, models 1 and 3 predict significantly higher degrees of polarization than models 2 and 4 for wavelengths longer than about  $200 \mu\text{m}$ . For example, when  $\lambda = 3000 \mu\text{m}$ , the maximum degree of polarization predicted by models 1 and 3 is of order 10%, while models 2 and 4 lead to a maximum of about 15%. These differences provide another way of discriminating between dust models, this time from observations of the polarized emission from interstellar dust.

The strong wavelength-dependence of the polarization in models 1 and 3 can be easily understood. In these two models, the carbonaceous grains are not aligned. For the adopted grain optical properties, the silicate grains contribute an increasing fraction of the emission as the wavelength increases, in part because the silicate grains are slightly cooler than the carbonaceous grains (this explains the behavior at  $\lambda \lesssim 200 \mu\text{m}$ ), and in part because the ratio of the silicate opacity to the graphite opacity increases with increasing wavelength for  $\lambda \gtrsim 100 \mu\text{m}$ .

## 9. SUMMARY AND FURTHER DISCUSSION

The main results of this paper are as follows:

1. We present models of interstellar dust based on

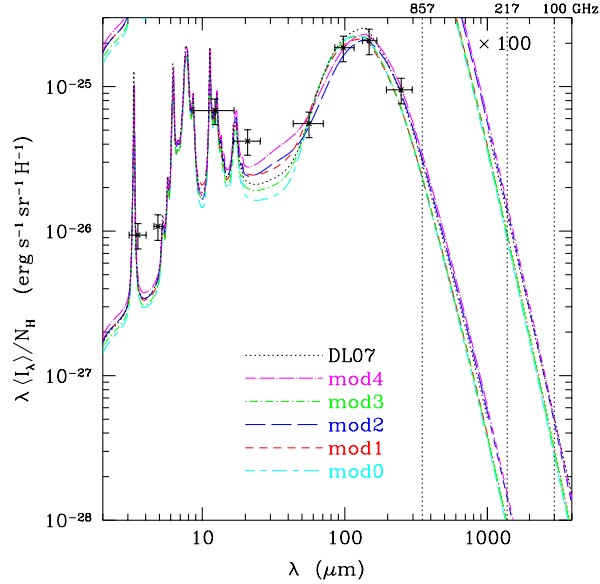


FIG. 7.— Total emission spectra for the different grain models listed in Table 1, as well as for the model described in Draine & Li (2007), each heated by the interstellar radiation field estimated by Mathis et al. (1983). The  $x$ -axis is now labeled by wavelengths, and the symbols correspond to the DIRBE results for HI correlated emission at high Galactic latitudes (Dwek et al. 1997; Arendt et al. 1998). Frequencies covering the full range of *Planck* HFI frequencies (100 GHz, 217 GHz, and 857 GHz) are also indicated.

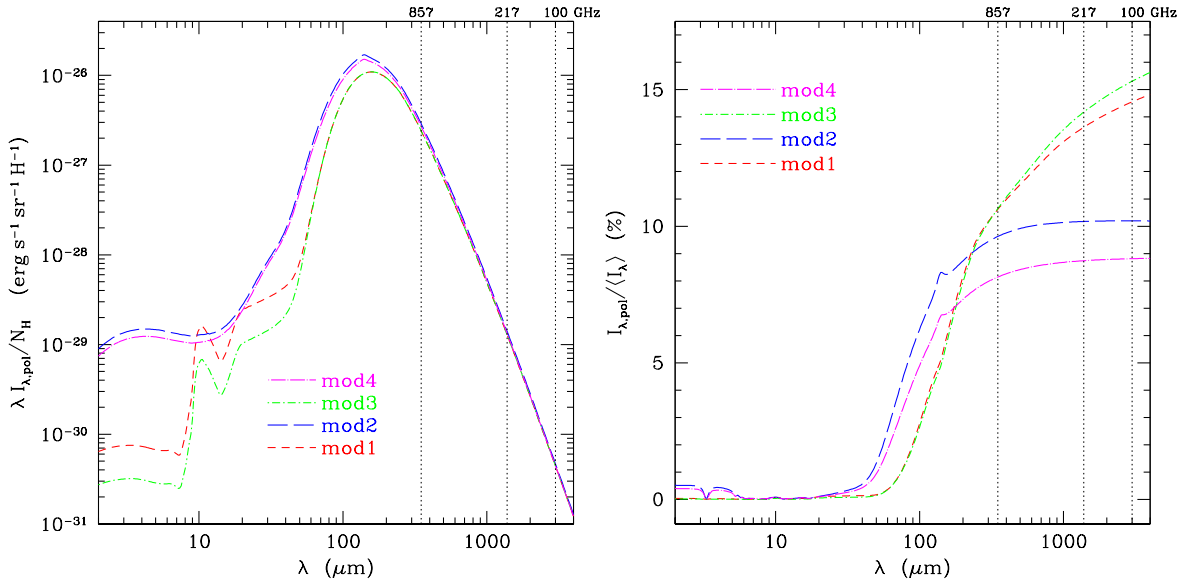


FIG. 8.— (*Left*) Spectra of polarized thermal emission predicted by models 1 through 4 in directions perpendicular to the direction of the local magnetic field, and (*Right*) corresponding degrees of polarization for each model. Two classes of models are clearly visible. Note that these models do not include rotational emission from spinning dust, which will be important for  $\lambda \gtrsim 4000 \mu\text{m}$  ( $\nu \lesssim 75 \text{ GHz}$ ).

- mixtures of spheroidal amorphous silicate grains, spheroidal graphite grains, and PAH particles, with a degree of alignment  $f$  that is a function of the effective radius  $a_{\text{eff}}$  of the grains. The models differ in assumptions concerning the shapes (axial ratios  $b/a = 1.4$  and  $1.6$  are considered for the spheroidal grains) of the silicate and graphite grains.
- Size distributions  $dn/da_{\text{eff}}$  and alignment function  $f(a_{\text{eff}})$  are found that reproduce the observed wavelength-dependent extinction and polarization of starlight. As found previously by Kim & Martin

(1995), the degree of alignment is small for  $a_{\text{eff}} \lesssim 0.05 \mu\text{m}$ , and large for  $a_{\text{eff}} \gtrsim 0.1 \mu\text{m}$ .

- For models where only the silicate grains are aligned, the degree of alignment approaches 100% for  $a \gtrsim 0.1 \mu\text{m}$ , whereas when both silicate and graphite grains are partially-aligned spheroids with  $b/a = 1.4$ , the observed starlight polarization can be reproduced with  $f \approx 0.4$  for  $a \gtrsim 0.1 \mu\text{m}$ . If the axial ratio is increased to  $b/a = 1.6$ , the required degree of alignment drops to  $f \approx 0.3$ .
- For each model, we calculate the partially-polarized

infrared emission when the dust is illuminated by the local starlight background. The total infrared emission spectra are generally similar, and in approximate agreement with observations of the Galactic cirrus emission at  $|b| \gtrsim 20^\circ$ . In detail, the spectra are model-dependent, particularly between about  $20 \mu\text{m}$  and  $160 \mu\text{m}$ . No attempt has been made to adjust our models to reproduce observed FIR spectral energy distributions.

5. Because the small grains and PAHs are not aligned, the polarized emission is very weak for  $\lambda \lesssim 40 \mu\text{m}$ . However, for  $\lambda \gtrsim 60 \mu\text{m}$ , the linear polarization of the thermal emission is appreciable when viewed from directions perpendicular to the local magnetic field. At  $100 \mu\text{m}$ , the different models considered here result in linear polarizations between about 3% and 6%. For wavelengths longer than  $500 \mu\text{m}$  ( $\nu \leq 600 \text{ GHz}$ ), of relevance to CMB studies, the degrees of polarization predicted by our models range from about 9% to around 15% for the thermal emission. However, for  $\lambda \gtrsim 4000 \mu\text{m}$  ( $\nu \lesssim 75 \text{ GHz}$ ), one should take into account the additional emission from spinning dust, which is not included here. This rotational emission is expected to be nearly unpolarized (Lazarian & Draine 2000), which will lower the overall polarization.
6. For models that employ more than one type of grain, which is the case of all our models, their relative contribution to the far-infrared and submillimeter emission will in general vary with wavelength. If the two types of grain have different values of  $C_{\text{pol}}/C_{\text{abs}}$  because of different alignment fractions or grain properties, the degree of polarization will vary with wavelength. This effect is very pronounced in our models 1 and 3 where only the

silicate grains are aligned with the magnetic field.

These last two results are particularly interesting for studies of the polarized components of the CMB. Polarized dust emission is indeed one of the brightest Galactic foregrounds at microwave frequencies, and being able to remove it from Galactic maps is one of the biggest challenges that will limit our ability to detect B-modes.

The maximum degrees of polarization we calculated in §8 are consistent with the level inferred from the *WMAP* observations (Page et al. 2007; Gold et al. 2008), although 5% is on the lower side of our predictions. Upcoming experiments, such as *Planck*, might therefore want to allow for the possibility of dust polarization being slightly higher in their sky models, and consider how this would affect their ability to constrain E- and B-modes.

More important is the possible wavelength-dependence of the degree of polarized dust emission. Models involving both silicate and carbonaceous spheroidal grains lead to a roughly constant level of polarization at all *Planck* frequencies. However, there is currently no evidence that carbonaceous dust grains contribute to the polarized signal at any wavelength, and models where only silicate grains are aligned spheroids lead to degrees of polarization that are strongly frequency-dependent. Although a possible challenge for the CMB community, this will allow the use of *Planck* observations to test whether the submm emission arises from a single kind of grain or from multiple grain types having different values of  $C_{\text{pol}}/C_{\text{abs}}$ .

This work was supported in part by NSF grant AST-0406883. AAF was additionally supported by Princeton University and NSF grant AST-0707932. The authors thank R. H. Lupton for making the SM package available to them. This research has made use of NASA's Astrophysics Data System Bibliographic Services.

## REFERENCES

- Anderson, C. M. et al. 1996, *AJ*, 112, 2726  
 Arendt, R. G. et al. 1998, *ApJ*, 508, 74  
 Asplund, M. 2000, *A&A*, 359, 755  
 Asplund, M., Grevesse, N., Sauval, A. J., Allende Prieto, C., & Blomme, R. 2005, *A&A*, 431, 693  
 Barnard, E. E. 1907, *ApJ*, 25, 218  
 ——. 1910, *ApJ*, 31, 8  
 Benoît, A. et al. 2004, *A&A*, 424, 571  
 Bohlin, R. C., Savage, B. D., & Drake, J. F. 1978, *ApJ*, 224, 132  
 Bohren, C. F., & Huffman, D. R. 1983, *Absorption and Scattering of Light by Small Particles* (New York: Wiley)  
 Cardelli, J. A., Mathis, J. S., Ebbets, D. C., & Savage, B. D. 1993, *ApJ*, 402, L17  
 Centeno, R., & Socas-Navarro, H. 2008, *ApJ*, 682, L61  
 Chiar, J. E. et al. 2006, *ApJ*, 651, 268  
 Clayton, G. C. et al. 1992, *ApJ*, 385, L53  
 Draine, B. T. 2003, *ARA&A*, 41, 241  
 Draine, B. T., & Allaf-Akbari, K. 2006, *ApJ*, 652, 1318  
 Draine, B. T., & Lazarian, A. 1998, *ApJ*, 494, L19  
 Draine, B. T., & Li, A. 2007, *ApJ*, 657, 810  
 Draine, B. T., & Malhotra, S. 1993, *ApJ*, 414, 632  
 Dwek, E. et al. 1997, *ApJ*, 475, 565  
 Finkbeiner, D. P. 2004, *ApJ*, 614, 186  
 Fitzpatrick, E. L. 1999, *PASP*, 111, 63  
 Fitzpatrick, E. L. 2004, in *Astrophysics of Dust*, ed. A. N. Witt, G. C. Clayton, & B. T. Draine, ASP Conference Series 309, 33  
 Flaherty, K. M., Pipher, J. L., Megeath, S. T., Winston, E. M., Gutermuth, R. A., Muzerolle, J., Allen, L. E., & Fazio, G. G. 2007, *ApJ*, 663, 1069  
 Gold, B. et al. 2008, ArXiv e-prints, 0803.0715  
 Grevesse, N., & Sauval, A. J. 1998, *Space Science Reviews*, 85, 161  
 Hall, J. S. 1949, *Science*, 109, 166  
 Hildebrand, R. 2005, in *Astronomical Polarimetry: Current Status and Future Directions*, ed. A. Adamson, C. Aspin, C. Davis, & T. Fujiyoshi, ASP Conference Series 343, 515  
 Hildebrand, R., & Kirby, L. 2004, in *Astrophysics of Dust*, ed. A. N. Witt, G. C. Clayton, & B. T. Draine, ASP Conference Series 309, 515  
 Hiltner, W. A. 1949, *Science*, 109, 165  
 Indebetouw, R. et al. 2005, *ApJ*, 619, 931  
 Jenkins, E. B. 2004, in *Origin and Evolution of the Elements*, ed. A. McWilliam & M. Rauch, 336  
 Kim, S.-H., & Martin, P. G. 1995, *ApJ*, 444, 293  
 Landi, E., Feldman, U., & Doschek, G. A. 2007, *ApJ*, 659, 743  
 Lazarian, A., & Draine, B. T. 1999, *ApJ*, 520, L67  
 ——. 2000, *ApJ*, 536, L15  
 Li, A., & Draine, B. T. 2001, *ApJ*, 554, 778  
 Lutz, D. et al. 1996, *A&A*, 315, L269  
 Martin, P. G. et al. 1992, *ApJ*, 392, 691  
 Martin, P. G., Clayton, G. C., & Wolff, M. J. 1999, *ApJ*, 510, 905  
 Mathis, J. S., Mezger, P. G., & Panagia, N. 1983, *A&A*, 128, 212  
 Mishchenko, M. I. 2000, *Appl. Opt.*, 39, 1026  
 Mishchenko, M. I., & Travis, L. D. 1994, *Opt. Comm.*, 109, 16  
 Nishiyama, S. et al. 2006, *ApJ*, 638, 839  
 Page, L. et al. 2007, *ApJS*, 170, 335  
 Pendleton, Y. J., & Allamandola, L. J. 2002, *ApJS*, 138, 75  
 Ponthieu, N. et al. 2005, *A&A*, 444, 327

- Roberge, W. G. 2004, in *Astrophysics of Dust*, ed. A. N. Witt, G. C. Clayton, & B. T. Draine, ASP Conference Series 309, 467
- Rosenthal, D., Bertoldi, F., & Drapatz, S. 2000, *A&A*, 356, 705
- Serkowski, K. 1973, in *Interstellar Dust and Related Topics*, ed. J. M. Greenberg & H. C. van de Hulst, IAU Symposium 52, 145
- Smith, C. H., Wright, C. M., Aitken, D. K., Roche, P. F., & Hough, J. H. 2000, *MNRAS*, 312, 327
- Trumpler, R. J. 1930, *PASP*, 42, 214
- Vaillancourt, J. E. 2002, *ApJS*, 142, 53
- Vaillancourt, J. E. 2007, in *EAS Publications Series 23*, 147
- Waterman, P. C. 1971, *Phys. Rev. D*, 3, 825
- Weingartner, J. C., & Draine, B. T. 2001, *ApJ*, 548, 296
- Whittet, D. C. B. 2003, *Dust in the Galactic Environment* (Bristol: Institute of Physics (IOP) Publishing)
- Wielaard, D. J., Mishchenko, M. I., Macke, A., & Carlson, B. E. 1997, *Appl. Opt.*, 36, 4305
- Wolff, M. J., Clayton, G. C., Kim, S.-H., Martin, P. G., & Anderson, C. M. 1997, *ApJ*, 478, 395